Effect of Casting Diameter and Heat Treatment Process on Microstructural Evolution and Mechanical Properties of $Fe_{55-X}Cr_{18}Mo_7B_{16}C_4Nb_X$ (X=0,3) Ribbons and Nanostructured Rods

M. Tavakoli Harandi[1] , M. Askari-Paykani[1] , H. Shahverdi[1,*] and M. Nili Ahmadabadi[2,3]

[*] *Shahverdi@modares.ac.ir*

Received: February 2018 **Revised: August 2018** **Accepted: January 2019**

[1] Tarbiat Modares University, Department of Materials Engineering, Tehran, Iran.

[2] School of Metallurgy and Materials Engineering, College of Engineering, University of Tehran, North Kargar Street, Tehran, Iran.

[3] Center of Excellence for High Performance Materials, School of Metallurgy and Materials Engineering, College of Engineering, University of Tehran, Tehran, Iran.

DOI: 10.22068/ijmse.16.1.68

Abstract: *One-step and two-step annealing techniques were used to examine the relationship between microstructure and mechanical properties during compression tests in iron-based ribbons and nanostructured 1- and 2.5mm cylindrical rods. The X-ray diffraction, microstructural, and mechanical results showed that substituting Nb for Fe had a minor effect on glass-forming ability but it increased the formability index. The novel two-step annealing process resulted in a remarkable formability index of 16.62 GPa, yield stress of 2830 MPa, ultimate strength of 3866 MPa, and 4.3% plastic strain. A ductile nanosized α-Fe framework and boron-containing nano precipitations, which caused Zener pinning effect, were responsible for these novel mechanical properties.*

Keywords: *Casting, Rapid solidification, Heat treatment, Microstructure, Mechanical properties*

1. INTRODUCTION

Due to the unique properties of Fe-based (bulk) metallic glasses (BMGs/MGs), such as relatively low material cost, high strength and hardness values, enhanced corrosion resistance, and potential candidacy as precursors for nanocrystalline composite materials [1-3], a number of Fe-based MGs have recently been developed as potential engineering materials.

Crystallization of MGs, one of the recently developed methods of nanocrystalline material production, has been used successfully in various alloy systems, such as Fe-, Ni-, and Cu-based alloys [4-7]. Because the glass state is thermo-mechanically metastable, the crystallization driving force is very high [8]. If crystallization occurs at lower temperatures, diffusion is limited, resulting in a very high nucleation frequency with limited time for growth, which leads to the formation of nanoscale phases [9]. High-temperature crystallization (after the last crystallization event) before grain pinning, results in a high rate of grain growth [5]. To obtain a nanoscale structure, the high-temperature crystallization process should proceed with the largest nucleation rate possible while suppressing the crystal growth rate as much as practicable. Such conditions can be obtained by halting grain growth via low-temperature precipitation, which causes Zener pinning effect [10].

In this paper, the effects of low- and high-temperature annealing as well as casting cooling rate on microstructural evolution and the mechanical/microstructural relationship of a Fe-based MG and nanocrystalline counterpart were investigated. A novel heat treatment was applied to glassy ribbons and nanostructured cylindrical rods, resulting in a remarkable formability index and ductility. The motivation for this study came from study results that demonstrated that annealing as-cast BMGs can markedly alter their mechanical behavior [1-3].

[DOI: 10.22068/ijmse.16.1.68]

2. EXPERIMENTAL PROCEDURE

Fe-based multi-component master alloys with a nominal composition of $Fe_{55-x}Cr_{18}Mo_7B_{16}C_4Nb_X$ (X=0(MG-0), 3(MG-3)) were prepared by vacuum arc remelting in a water-cooled copper mold. Commercially pure Fe (99.7% purity), Cr (99.9% purity), Nb (99.9% purity), Mo (99.9% purity), B (99.9% purity), and C (99% purity) were used to prepare the master alloy ingots. In order to obtain more homogeneous structures, the ingots were remelted four times. Fe-based MG ribbons (60×800 μm) were produced using a melt-spinning technique; 15 g of the ingot were used for melt spinning each specimen. The melt-spun ribbons were formed by primary induction melting, followed by injecting the liquid melt onto a rapidly moving copper chill wheel. In the melt-spinning process, chamber pressure was 2.8×10^{-4} torr, tangential wheel velocity was 32.5 m/s, and melt injection pressure was 325 torr.

In order to investigate the effects of casting cooling rate on the microstructure evolution and mechanical properties of the alloys, 1×60 mm and 2.5×60 mm (diameter × length) cylindrical rods were produced by water-cooled copper mold suction casting. A PerkinElmer differential scanning calorimeter (DSC) was used at a heating rate of 10 K/min to verify the structure of the melt-spun ribbons and the thermal behavior related to the glass transition and crystallization temperatures. A NETZSCH differential thermal analyzer was used (DTA) at a heating rate of 10 K/min to determine melting event temperatures. The melt-spun ribbons and the 1×60 mm and 2.5×60 mm rods were isothermally annealed under a vacuum of 10^{-3} torr, according to the conditions shown in Table 2. A Philips X'Pert Pro X-ray diffractometer (XRD) using Cu-Kα (λ=0.1541 nm) was used to verify the microstructure evolutions through different casting cooling rates and heat treatment conditions. Room temperature uniaxial compression tests were carried out with an Instron-type universal testing machine at a strain rate of 10^{-4} s^{-1}. Compression specimens with two different diameters (1 and 2.5 mm) and an aspect ratio of 2:1 were cut from the cylindrical rods. In order to ensure that the results could be reproduced, mechanical tests were performed on three samples. The two ends of the test pieces were carefully polished to ensure parallel and flat surfaces. The fracture morphology and the microstructural changes of the rod specimens were studied with a Carl Zeiss Gemini field emission scanning electron microscope.

3. RESULTS AND DISCUSSION

3.1. Thermal Analysis

Fig. 1 and Table 1 show the DSC curves and extracted characterization temperatures of the as-spun MG-0 and MG-3 specimens. Here T_g , $T_{X1,}$ $T_{X2,}$ T_{X3} are glass transition, first, second and third crystallization temperatures, respectively.

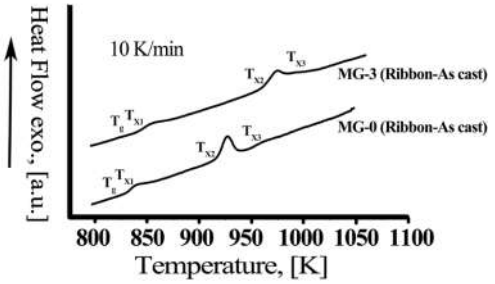

Fig.1. DSC curves of the melt-spun MG-0 and MG-3 specimens at 10 K/min.

3.2. Microstructural Evolutions

According to Fig. 1, the DSC measurement revealed one endothermic and three exothermic peaks corresponding to the glass transition (T_g) and crystallization ($T_{X1,2,3}$) events. The glass transition was followed by a super-cooled liquid region ($\Delta T_X=T_{X1}-T_g$) before crystallization, thus confirming that the MG-0 and MG-3 ribbons were amorphous. Fig. 2 shows the XRD patterns of the as-spun and annealed MG-0 and MG-3 specimens. The XRD patterns of the MG-0 and MG-3 ribbons (Figs. 2a and 2d) reveal only one typical diffuse peak (peaks corresponding to crystallization events are not visible), which also indicates that these specimens essentially consist of a single amorphous phase. The thermal properties of

[DOI: 10.22068/ijmse.16.1.68]

the as-spun MG-0 and MG-3 specimens are summarized in Table 1. The T_g - T_X intervals that of MG-0 and MG-3 specimens are 817–828 K and 832–1003 K, respectively;means super-cooled liquid intervals of 15 and 17 K, respectively. Furthermore,both T_g and T_X were increased gradually when 3 at.% Fe was replaced with Nb. The onset melting temperature (T_m), liquidus temperature (T_l), and reduced glass transition temperature (T_{rg}=T_g/T_l) are also included in Table 1. These temperatures and the interval between T_m and T_l weredecreased when Fe was replaced by Nb, brings the alloy close to a eutectic composition. The calculated T_{rg} values for the MG-0 and MG-3 ribbons were 0.52 and 0.53, respectively. These different thermal behaviors originate from Nb addition means that Nb increases the glass forming ability.

Glass-forming ability (GFA) can be evaluated from thermal stability measurements. As a rule of thumb, high ΔT_X and T_{rg} values are indicative of good GFA [11]. Using these values to predict

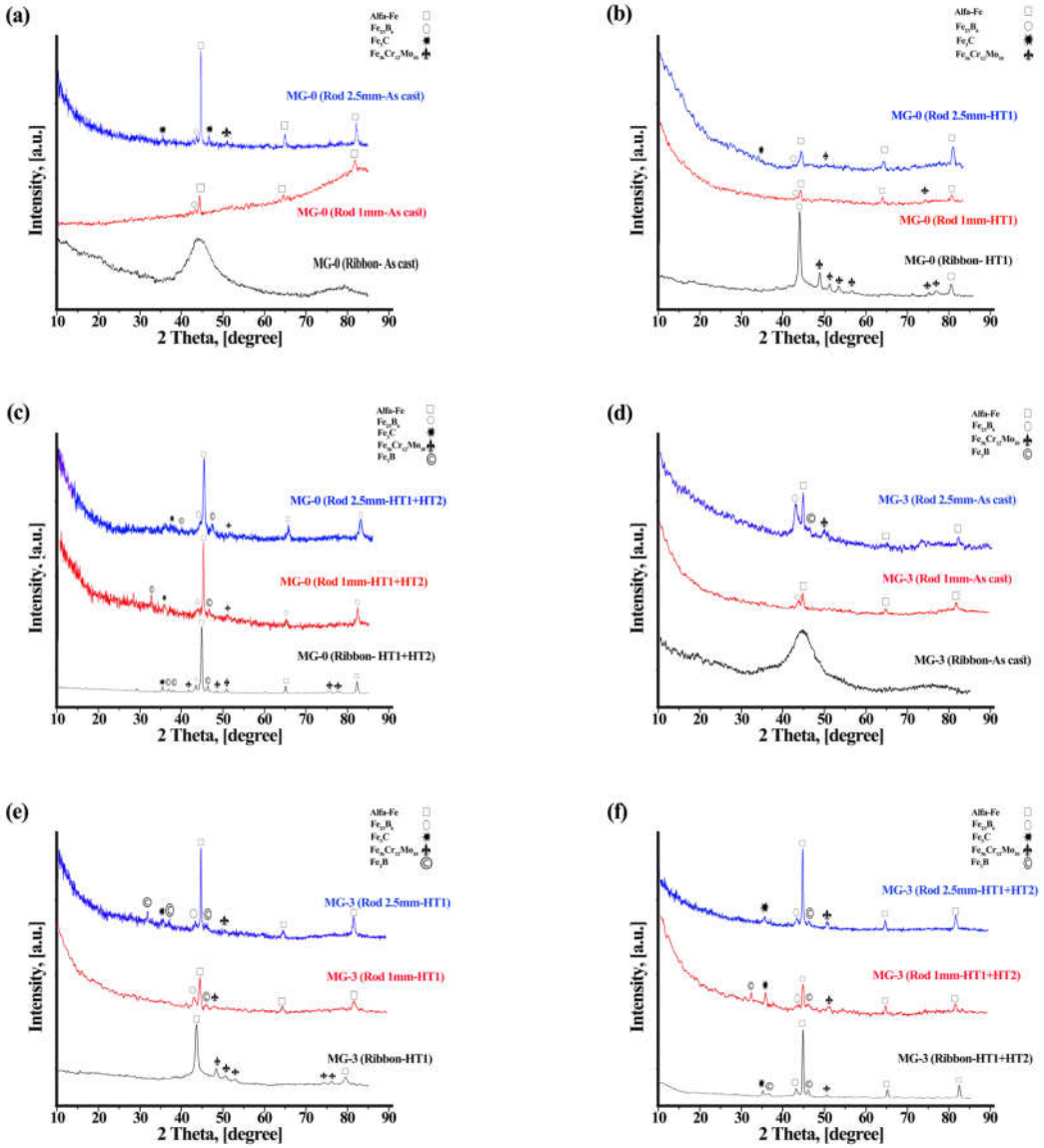

Fig.2. (a-c) XRD patterns of the as-cast and heat treated MG-0 (Fe55Cr18Mo7B16C4) and (d-f) XRD patterns of the as-cast and heat treated MG-3 (Fe52Cr18Mo7B16C4Nb3)

[DOI: 10.22068/ijmse.16.1.68]

the GFAs of various glass-forming systems, including MG-0 and MG-3 systems, and based on Inoue empirical criteria (deep eutectics) [12], substituting Nb for Fe enhances the GFA of the alloy. It is said that these amount of T_{rg} temperature shiftingf,i.e, ~0.53,is characteristic of a good Fe-based glass-forming system [11]; However, is still low compared to the amounts of 0.57–0.72 measured in two excellent glass-forming systems,i.e. $(Pd,Ni,Cu)_{80}P_{20}$ and $(Pd,Ni,Fe)_{80}P_{20}$ [13,14].

Regarding the effects of element substitution on GFA, it has been reported that the chemistry of the specimens is more effective than their atomic size [15]. This finding can be explained by the chemical structure of MGs. Chemical short-range order (CSRO) exists in the MGs , correlates to their GFA [16]. In a topological model for the formation of MGs, atomic size mismatch and the interactions between different atoms are crucial factors in forming topological constraints [17]. Similarly, the negative heat of mixing among main constituent elements is one of the three empirical rules [12]. According to the results of Ji and Yang [15], element substitution is able to enhance the GFA of MGs effectively, if the added elements have similar atomic sizes and chemical properties as the substituted element. Nb and Fe are not similar in chemical properties or atomic size; therefore, when Nb was added to the FeCrMoBC alloying system, its effect on GFA was negligible. On the other hand, MG formers must have good interaction and size arrangements between atom pairs or groups. Additional atoms will change the previous CSRO of a specific MG. Adding atoms cannot replace the position held by the substituted atoms, even if the added atoms are similar in size but have no similar interaction with other surrounding atoms [15]. Such elements will destroy the previous CSRO and won't be suitable for GFA. Based on the confusion principle [12],if the added atoms are not similar in size the interaction of atomic pairs or groups could still result in holding the old positions of the substituted atoms. Therefore, the old CSRO is retained, and such substitutions will improve the GFA. However, it appears that the confusion principal outweighs the chemical interaction of atoms, resulting in some minor beneficial changes in the GFA of the Fe-CrMoBC alloy system.

Ribbon specimens in the as-cast state were annealed for 100 h at temperatures below T_g (T_g-30). These specimens coded as HT1 . The HT1 specimens were also subjected to isothermal heating above T_{P3} (T_{P3}+15) in the third crystallization event for one hour.. These specimens were labeled HT1+HT2 specimens.. The XRD data of the as-spun and annealed ribbons, as well as the rods in as-cast and annealed states, are shown in Fig. 2. It can be seen that the as-cast 1 and 2.5mm-diameter rods are not amorphous and some crystallites of α-Fe, $Fe_{23}B_6$, Fe_3C and $Fe_{36}Cr_{12}Mo_{10}$ are present in their patterns. As it was shown previously, MG-0 and MG-3 ribbons show an onset of crystallization (T_{X1}) at 832 K and 845 K, respectively, (Fig. 1, Table 1). Annealing of the specimens for 100 h at T_g-30, results in crystallization of only $Fe_{36}Cr_{12}Mo_{10}$ (Fig. 2).

When an amorphous material is heat-treated at a temperature below T_g, the structure of the glassy material tends toward a more stable state; however, crystallization will occur only if the heat treatment time be enough [18]. This phenomenon, known as structural relaxation, has been observed in a variety of amorphous materials, including MGs, polymers, and oxide glasses [19,20]. In some MGs, reversible or irreversible phenomena can occur during structural relaxation, which can be attributed to modifications in the topological range order or variations in the CSRO [21]. The nature of the transformation of the amorphous structure depends on the temperature at which the glass is annealed and the types of constituents present in the alloy system [22]. If annealing is carried out at a very low temperature with respect to T_{X1}, its crystallization may take an unusually long time, and not on a timescale where experimental observations can be made [22]. As shown in Figs. 2 and 3, using a low temperature and a long time (T_g-30, 100h) for the HT1 annealing process causes some nanocrystallization events. Zhang et al. [23] also reported that some crystallization peaks appeared after annealing a Fe-based system below the T_{X1} temperature.

When the specimens were annealed at (T_{P3}+15), which is higher than T_{X3}, some new phases were identified as $Fe_{23}B_6$, Fe_3B, and Fe_3C (Fig. 2). It was also confirmed that after the Nb

[DOI: 10.22068/ijmse.16.1.68]

substitution, the structure consisted of fewer α-Fe and Fe_3C phases and more $Fe_{23}B_6$ associated with the appearance of Fe_3B. The metastable α-Fe and Fe_3C phases were decomposed in the final crystallization process, and Nb promoted the formation of boron-containing phases. Therefore, the phase transformation behavior of the FeCrMoBC alloy system with Nb substitution can be summarized as follows:

α-Fe partially decomposes and Fe_3C fully decomposesd lead to precipitation of $Fe_{23}B_6$ and Fe_3B phases.

Based on these results, the substitution of 3 at.% of Nb into the FeCrMoBC alloy system leads to the precipitation of boron-containing phases during the annealing and/or casting of rods with different diameters (i.e., different cooling rates). The main boron-containing phase in the FeCrMoBCNb glassy alloy is the $Fe_{23}B_6$ phase. It is known that $Fe_{23}B_6$ has a complex FCC structure, with a lattice parameter as large as 1 nm comprising 96 atoms. Its precipitation from the network-like glassy structure requires long-range atomic rearrangements of constituent elements, which leads to the high stability of the supercooled liquid and consequently, to a high GFA [24]. Mo and Nb are in a periodic table group and are similar in terms of atomic radius, mixing enthalpies, and electronic structure. Therefore, for better GFA, Mo is a more appropriate choice as a substitute than Nb.

The sizes of the phases were analyzed with a microstructural image analyzer (MIP image analyzer processor) (Fig. 3). The main phases in t HT1 after annealing, which were α-Fe (Figs. 2 and 3a), had a length e of 75±12 nm, while heat treatment of HT2caused coarsening of the grains to 195±17 nm (Fig. 3b). Annealing of HT1+HT2 also caused the precipitation of some nanoscaled phases, which were mainly boron-containing compounds (Figs. 2 and 3b). During the the low temperature annealing(T_g-30) of HT1 the α-Fe phase formed preferentially , due to the hyperstoichiometric concentration of Fe in the amorphous phase compared with the other precipitation phases. The growth of the α-Fe phase was consequently restricted by the limited mobility of Fe at this low annealing temperature. However, during the HT1+HT2 annealing treatment, the redistribution of C and B caused locally stoichiometric $Fe_{23}B_6$ and Fe_3B phases to form, as well as the nucleation and growth of these phases. The size of these Fe_3B and $Fe_{23}B_6$ subgrains was limited to the nanometer range (Fig. 3). These phases appeared to behave as Zener pinning sites that can limit grain growth during high-temperature annealing [10].

3.3. Mechanical Properties

Fig. 4 shows the compressive stress-strain curves and Table 3 summarizes the compressive test results, including yield stress (σ_Y), ultimate strength (σ_{Max}), plastic strain (%), and index of formability ($\sigma_{Max}\times$%). The 1- and 2.5 mm rods began to yield at 1170–4230 MPa, followed by different degrees of plastic strain prior to failure. In all of the specimens, as the Nb content increased from 0 to 3 at%, the yield and ultimate strength increased, while the plasticity exhibited a

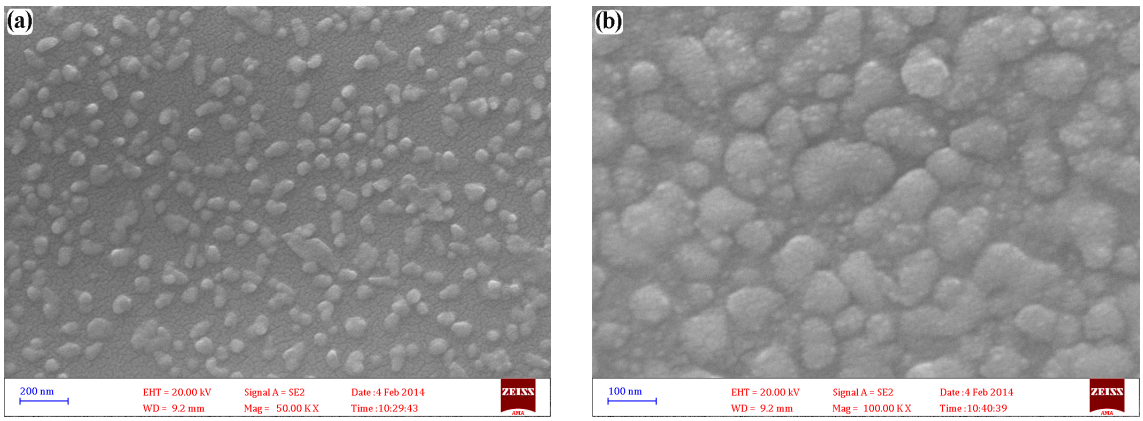

Fig. 3. Microstructure of (a) MG-3 (Ribbon-HT1) and (b) MG-3 (Ribbon-HT1+HT2).

[DOI: 10.22068/ijmse.16.1.68]

gradual decrease. It is obvious that after the HT1 annealing process, the specimens showed an improvement in plastic strain, while the HT1+HT2 heat-treated specimens showed a major increase in el%. As an index of the formability and absorbed energy of materials, the product of ultimate strength (σ_{Max}) and plastic strain (%), $\sigma_{Max}\times\%$, has been used to tailor steels roughly for automotive applications [26]. It is clear that HT1, and especially the HT1+HT2 annealing process, improved the formability index of all of the specimens. The Nb substitution only improved the index of formability in the 1mm cylindrical rods; the best index in the 1mm cylindrical rod was 16.62 GPa. % with 3 at.% Nb in the HT1+HT2 state.

Fig. 5 shows the fracture surfaces of the specimens after fracture; it can be seen that many slip bands (Figs. 5a and 5b) developed in the fracture surfaces. The river-like pattern (Figs. 5d and 5f) is a typical rod specimen fracture surface, caused by the adiabatic thermal process of slip bands. The rough surface was composed of slip bands areas, and the friction between two fracture surfaces during compressive deformation was responsible for the formation of smooth areas [26]. The same fracture features were observed on the all areas of the surfaces of the whole specimens, suggesting that the whole specimens experienced homogenous plastic deformation instead of rapid localized failure. The resultant microstructures consisted of different stiff (Fe_3C, $Fe_{23}B_6$, Fe_3B,…) and ductile (α-Fe) crystalline phases; therefore, deformation behavior and mechanical properties are related to its constituents. On the other hand, the plastic deformation of the rod specimens is related to the competition between the strain hardening of soft phases and the damage that may be induced in the hard phases. In the early stage of deformation, the α-Fe soft phase, with a lower elastic modulus, yielded under the dislocation motions, resulting in stress concentrations near interfaces. After yielding, dislocations formed preferentially from these stress-concentrated interfaces. The hard phases balanced the dislocation motion of the soft α-Fe

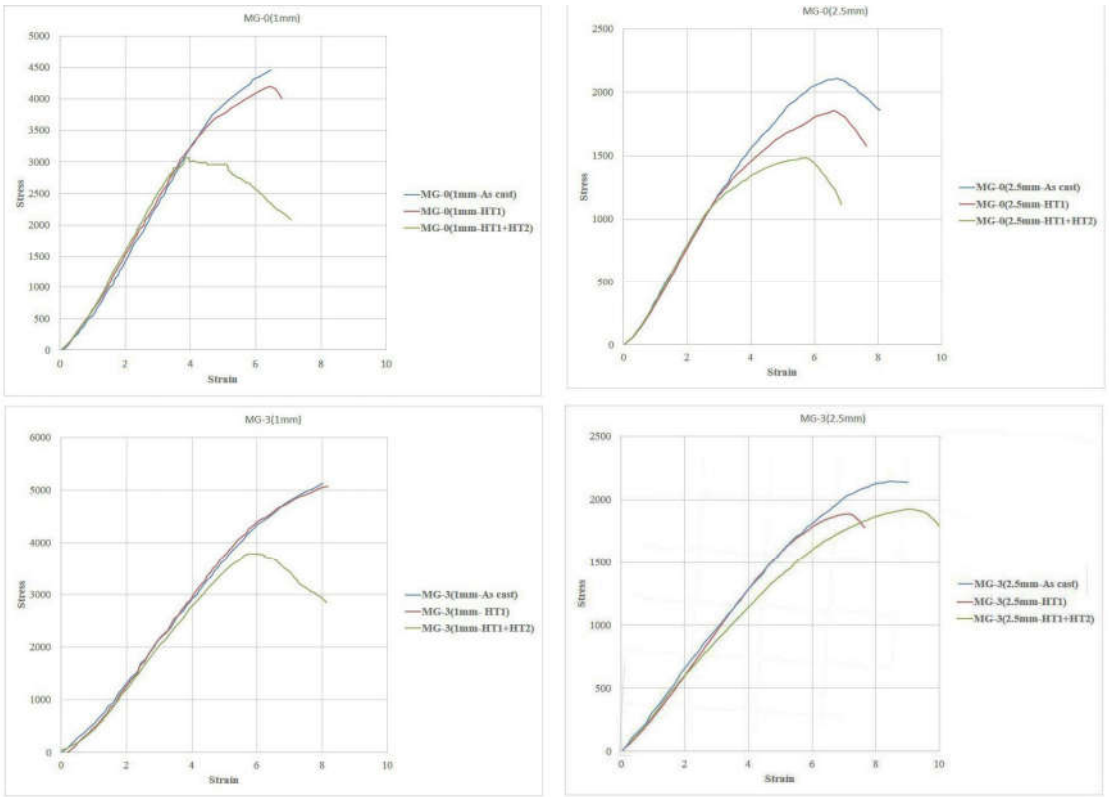

Fig. 4. Compressive stress- strain curves

[DOI: 10.22068/ijmse.16.1.68]

phase, which acted as a ductile framework (α-Fe was the main formed phase in all the specimens). As such, this microstructure, containing very fine, soft, and hard phases, exhibited a high degree of plasticity and a high formability index, as shown in Table 3. The Zener pinning effect of nanosized precipitation phases is another effective mechanism used to achieve good ductility. Compared with this structure, coarsening of the α-Fe (ductile framework role), changing the phase volume percentage, and additional phase precipitation as a result of different diameter rod casting (different cooling rates) and heat treatment processes cannot effectively balance the propagation of the dislocations, resulting in catastrophic failure.

On the basis of these investigations of microstructures and mechanical properties, it is evident that plasticity correlates closely with precipitated phases during HT1 and HT1+HT2 annealing processes. The boron-containing nanoparticles appeared to behave as Zener pinning sites that can serve to limit grain growth during high-temperature annealing processes.

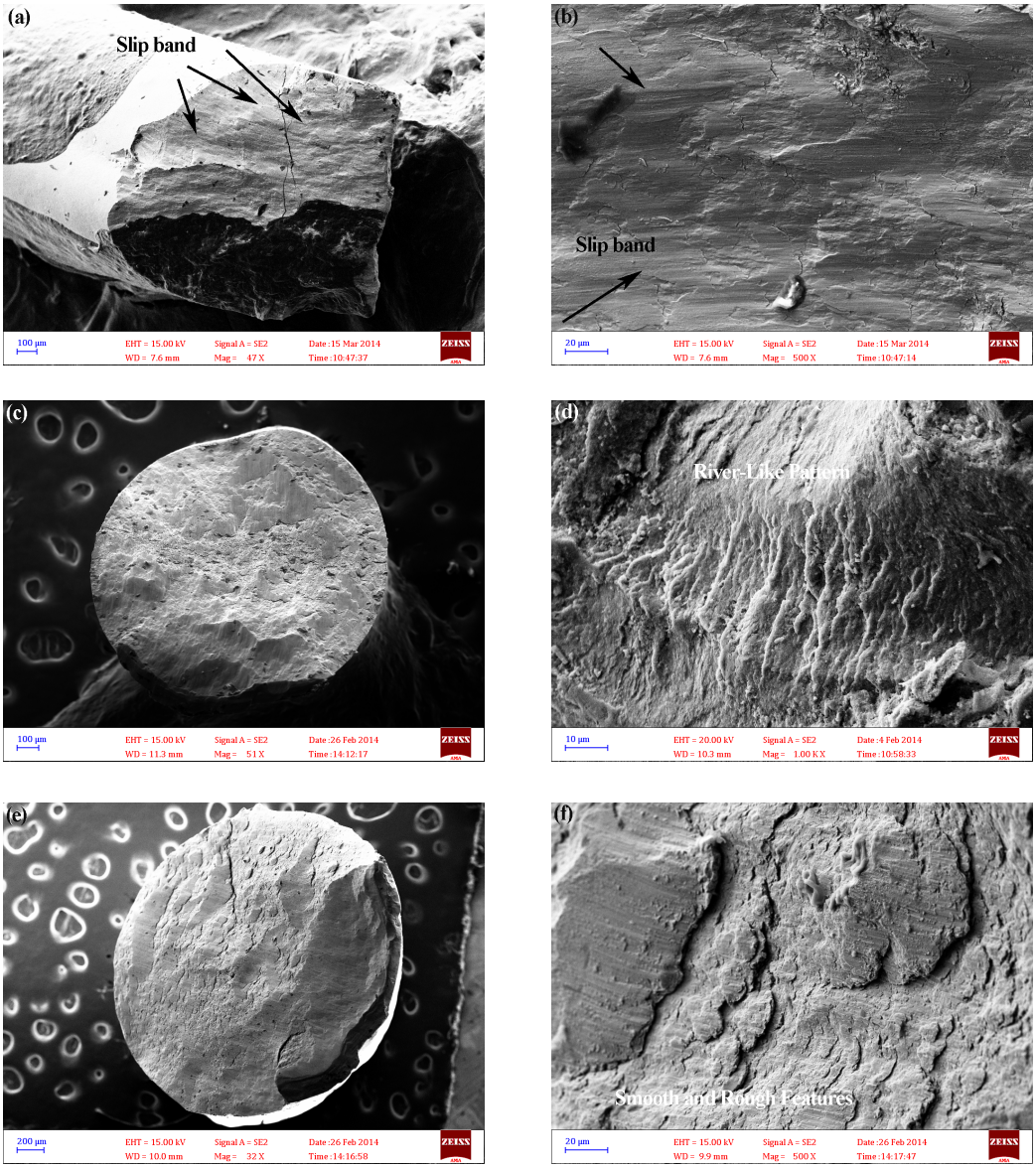

Fig. 5. Fracture surfaces of the rod specimens after compression tests: (a,b) MG-0 (1mm-As cast), (c,d) MG-0 (1mm- HT1+HT2), (e,f) MG-0 (2.5mm, As cast)

[DOI: 10.22068/ijmse.16.1.68]

4. CONCLUSIONS

In this study, $Fe_{55-x}Cr_{18}Mo_7B_{16}C_4Nb_X$ (x=0,3) ribbons and cylindrical rods in as-cast and one-step and two-step annealing states were analyzed to characterize their mechanical and microstructural evolutions. The results showed that a composite microstructure containing a ductile framework and Zener pinning precipitations had very novel mechanical properties: index of formability of 3–16 GPa%, yield stress of 1000–4000 MPa, and ultimate strength of 1400–4400 MPa.

REFERENCES

1. Seifoddini, A., Stoica, M., Nili-Ahmadabadi, M., Heshmati-Manesh, S., Kuhn, U. and Eckert, J., "New $(Fe_{0.9}Ni_{0.1})77Mo_5P_9C_{7.5}B_{1.5}$ glassy alloys with enhanced glass-forming ability and large compressive strain. Mater". Sci. Eng. A, 2013, 560, 575-582.
2. Askari-Paykani, M., NiliAhmadabadi, M., Seiffodini, A., "The effect of liquid phase separation on the Vickers microindentation shear bands evolution in a Fe-based bulk metallic glass". Mater. Sci. Eng. A, 2013, 585, 363-370.
3. Askari-Paykani, M., Nili-Ahmadabadi, M., Seiffodini, A., "On the subsurface deformation of two different Fe-based bulk metallic glasses indented by Vickers micro hardness", Intermetallics, 2014, 46, 118-125.
4. Branagan, D. J., Tang, Y., "Developing extra hardness (>15GPa) in Iron based nano composite". Composites: A. 2002, 33, 855-859.
5. Sergueeva, A. V., Mara, N. A. Branagan, D. J., Mukherjee, A. K., "Phase morphology effect on elevated temperature mechanical behavior of nanostructures", Mater. Let. 2007, 61, 1465–1468.
6. Li, H. F., Ramanujan, R. V., "Crystallization behavior of the cobalt based metallic glass $Co_{65}Si_{15}B_{14}Fe4Ni_2$", Mater. Sci. Eng. A. 2004, 375–377, 1087–1091.
7. Concustell, A., Alcala, G., Mato, S., Woodcock, T. G., Gebert, A., Eckert, J., Baro, M. D., "Effect of relaxation and primary nanocrystallization on the mechanical properties of $Cu_{60}Zr_{22}Ti_{18}$ bulk metallic glass". Intermetallics, 2005, 13, 1214–1219.
8. Minic, D. M., Minic, D. M., Zak, T., Roupcova P., David, B., "Structural transformations of $Fe_{81}B_{13}Si_4C_2$ amorphous alloy induced by heating". J. of Magn. Magn. Mater. 2011, 323, 400-404.
9. Louzguine-Luzgin, D. V., Seki, I., Wada, T., Inoue, A., "Structural Relaxation, Glass Transition, Viscous Formability, and Crystallization of Zr-Cu–Based Bulk Metallic Glasses on Heating, Metall. Mater. Trans". A. 2012, 43A, 2642-2648.
10. Humphreys, F. J., Ardakani, M. G., "Grain Boundary Migration and Zener Pinning in Particle-Containing Copper Crystals", Acta Mater. 1996, 44, 2711-2121.
11. Stoica, M., Eckert, J., Roth, S., Yavari, A. R., Schultz, L., "$Fe_{65.5}Cr_4Mo_4Ga_4P_{12}C_5B_{5.5}$ BMGs: Sample preparation, thermal stability and mechanical properties", J. Alloys Comp. 2007, 434–435, 171–175.
12. Inoue, A. "Bulk Amorphous Alloys: Preparation and Fundamental Characteristics; Vol. 4 of Materials Science Foundations". Uetikon-Zürich, Switzerland: Trans Tech Publications (1998).
13. Schwarz, R. B., He, Y., "Formation and properties of bulk amorphous Pd-Ni-P Alloys", Mater. Sci. Forum. 1997, 235–238, 231-240.
14. Shen, T. D., He, Y., Schwarz, R. B., "Bulk amorphous Pd–Ni–Fe–P alloys: Preparation and characterization", J. Mater. Res. 1999, 14, 2107-2115.
15. Ji, X. L., Yang, S. Z., "Enhanced glass forming ability of Fe-based alloys with minor additions". Front. Mater. Sci. China. 2010, 4, 411–414.
16. Chen, G. L., Hui, X. D., Fan, S. W., Kou., H., Yao., K., "Concept of chemical short range order domain and the glass forming ability in multicomponent liquid". Intermetallics 2002, 10, 1221–1232.
17. Zhang, J., Tan, H., Feng, Y. P., Li, Y., "The effect of Y on glass forming ability". Scripta Mater., 2005, 53, 183-187.
18. Qiao, J. C., Pelletier, J. M., "Enthalpy relaxation in $Cu_{46}Zr_{45}Al_7Y_2$ and $Zr_{55}Cu_{30}Ni_5A_{110}$ bulk metallic glasses by differential scanning calorimetry (DSC)". Intermetallics 2011, 19, 9-18.
19. Malek, J., Svoboda, R., Pustkova, P., Cicmanec, P., "Volume and enthalpy relaxation of a-Se in the glass transition region", J. Non-Cryst. Solids. 2009, 355, 264-272.
20. Pelletier, J. M., "Influence of structural relaxation on atomic mobility in a $Zr_{41.2}Ti_{13.8}Cu_{125}Ni_{10.0}Be_{22.5}$ (Vit1) bulk metallic glass", J. Non-Cryst Solids. 2008, 354, 3666-3670.
21. Pelletier, J. M., Moortèle V. D., "Phase separation and crystallization in the Zr41.2–Ti13.8–Cu12.5–Ni10–Be22.5 bulk metallic glass determined by physical measurements and electron microscopy", J. Non-Cryst Solids. 2003, 325, 133-141.

[DOI: 10.22068/ijmse.16.1.68]

22. Suryanarayana, C. and Inoue, A., "Bulk metallic glasses", Taylor and Francis Group, 2011, 118-200.
23. Zhang, J., Shen, B., Zhang, Z., "Crystallization behaviors of FeSiBPMo bulk metallic glasses", J. non-Crys. Solids. 2013, 360, 31-35.
24. Yoon, S., Kim, J., Bae, G., Kim, B., Lee, C., "Formation of coating and tribological behavior of kinetic sprayed Fe-based bulk metallic glass", J. Alloys Compd. 2011, 509, 347–353.
25. Demeri, M. Y., ""Advanced high strength steels: science", technology and applications, ASM International, 2013, 115-120.
26. Wu, F. F., Zhang. Z. F., Peker. A., Mao, S. X., Eckert, J., "Strength asymmetry of ductile dendrites reinforced Zr- and Ti-based composites", J. Mater. Res. 2006, 9, 2331-2336.

[DOI: 10.22068/ijmse.16.1.68]